

The Role of the Ocean in Midlatitude, Interannual-to-Decadal-Timescale Climate Variability of a Coupled Model

S. S. DRIJFHOUT, A. KATTENBERG, R. J. HAARSMA, AND F. M. SELTEN

Royal Netherlands Meteorological Institute, De Bilt, Netherlands

(Manuscript received 22 July 2000, in final form 12 February 2001)

ABSTRACT

Three 1000-yr climate simulations with an atmospheric general circulation model (AGCM) coupled to, respectively, a slab mixed layer model, an ocean GCM, and responding to yearly repeating daily sea surface temperature (SST) and sea-ice coverage climatology derived from the fully coupled run were analyzed and compared. When coupled to a slab mixed layer, surface air temperature (SAT) and SST are strongly coupled and the reddening is significantly larger than in the case of coupling to a dynamically active ocean. A simple one-dimensional stochastic model is developed to explain the different spectra of SAT above land and ocean. It is argued that ocean advection generating SST variability that does not match the principal modes of SAT above the ocean is the main factor in damping SAT variability. The variability of SAT and 800-hPa geopotential height (GEO) and covariability of SST–SAT and SST–GEO have been analyzed, and it is found that coupling does not change the dominant patterns of atmospheric variability, but it affects the spectra. The relative importance of the dominant patterns of variability is not affected by coupling, nor do significant peaks arise in the spectra. Coupling does give rise to preferred modes of *covariability* between SST and SAT or GEO. A dynamically active ocean affects the spectra of these modes and occasionally gives rise to a significant spectral peak on decadal to interdecadal timescales. Also, a dynamical ocean affects SAT spectra above sea by a systematic deviation from the fitted AR(1) process.

1. Introduction

The atmospheric global circulation is known to fluctuate on a vast range of timescales. Through the nonlinearity of the governing equations chaotic solutions are possible, which display variability with all kind of periods. James and James (1989, 1992) have demonstrated that major peaks at interannual and longer timescales are possible for a multilevel baroclinic atmospheric general circulation model. This low-frequency atmospheric variability is internal to the atmospheric flow; it is generated by the intrinsic instability of the mean flow and by the interactions among atmospheric flow structures at different spatial and temporal scales.

On the other hand, it is often surmised that the ocean is responsible for the “memory” of the climate system. Ocean processes, like the gyre circulation, water mass formation and the thermohaline circulation, are known to be associated with timescales of tens to hundreds of years. Their active or passive role in the climate system may give rise to such timescales in the observed variability of the climate. To assess the role of the ocean in creating the memory of the climate system on decadal

timescales, a simulation of atmospheric low-frequency variability by means of coupled ocean–atmospheric general circulation models is essential. This requires rather long runs (several hundreds to a thousand years) that have not been available until recently (Manabe and Stouffer 1996; Tett et al. 1997; von Storch et al. 1997; Gordon et al. 2000). These coupled models have been used to test, among others, several proposed mechanisms for low-frequency climate variability.

A rather well-established mechanism associated with low-frequency climate variability is the response of the ocean to atmospheric variations. Hasselmann (1976), validated by Frankignoul and Hasselmann (1977), showed that the ocean surface layers, due to their huge thermal inertia relative to the overlying atmosphere, integrate the rapidly varying (white noise) atmospheric changes and turn these into a slowly varying response. A red noise SST variability is expected and observed in regions away from intense currents and frontal systems in the ocean. The atmosphere, in its turn, will feel the slow SST variations and may show the lower frequencies too. This mechanism is also operating in coupled ocean–atmosphere climate models (Manabe and Stouffer 1996; Frankignoul et al. 1997).

A more subtle operation of the Hasselmann (1976) mechanism has been put forward by Barsugli (1995), who concluded that red noise SST variability acts to

Corresponding author address: S. S. Drijfhout, Royal Netherlands Meteorological Institute, P.O. Box 201, 3730 AE, De Bilt, Netherlands.
E-mail: drijfhout@knmi.nl

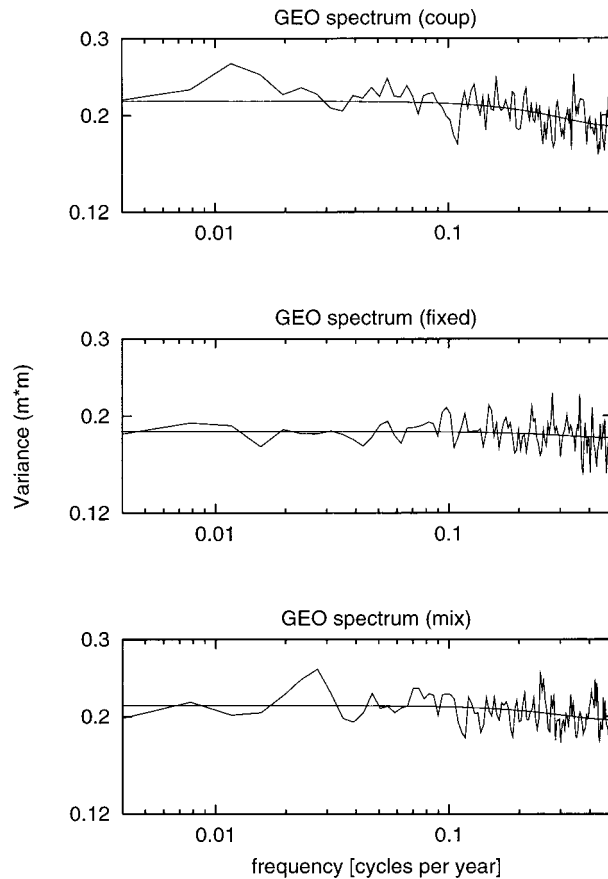


FIG. 1. Globally averaged spectra for the midlatitudes of yearly averaged GEO for the coupled, fixed SST and slab mixed layer runs, together with the fitted AR(1) process spectrum (m^2).

attenuate the damping of low-frequency atmospheric variability. He noted that the ocean does not imprint specific patterns of SST on the atmosphere, but merely changes the spectrum of the natural variability of surface air temperature (SAT) without affecting the preferred patterns. A confirmation of these ideas can be found in the studies of Delworth (1996), Saravanan and McWilliams (1997), and Bladé (1997). As a result, SST and atmospheric circulation anomalies can be significantly correlated, as the SST anomalies are driven by the atmosphere–ocean heat flux (Cayan 1992). In regions where ocean advection is important, ocean dynamics modify the ocean–atmosphere interaction by introducing preferred timescales of variability determined by the relevant ocean circulation timescale (Saravanan and McWilliams 1998).

Another way that low-frequency variability may arise in the climate system is when slow oceanic processes do imprint themselves on SST and by ocean–atmosphere interaction on the atmospheric conditions. For instance, an oscillatory ocean mode might be unstable and express itself even with steady forcing (Weaver and Sarachik 1991; Drijfhout et al. 1996). In some models, all such

oscillatory modes are damped and white noise atmospheric forcing is required to excite them (Mikolajewicz and Maier-Reimer 1990). The latter mechanism has also been identified in coupled models, (Delworth et al. 1993; Selten et al. 1999). Delworth et al. showed that interdecadal variations of the thermohaline circulation can generate anomalies of SST and SAT in the North Atlantic region similar to observed anomalies ascribed to such processes (Deser and Blackmon 1993; Kushnir 1994).

In some cases, it has been observed that the atmospheric response to midlatitude SST anomalies is significant (Ferranti et al. 1994), in other cases it was quite weak and inconsistent (Lau and Nath 1994). In this context, it has been surmised that transient eddy forcing plays a crucial role in determining the atmospheric response, which could explain the failure of low-resolution atmospheric models to exhibit a robust response to midlatitude SST anomalies (Kushnir and Held 1996).

A further mechanism for low-frequency climate variability to arise, is the possible existence of coupled ocean–atmosphere modes that require feedbacks between both media for their occurrence. Latif and Barnett (1996) describe such a mode in the North Pacific that they find in a 125-yr integration of a coupled model and in observed data. A similar mode in the North Atlantic has been found by Grötzner et al. (1998). In that study the covariability of SST with sea level pressure is similar to observed covariability with a 10–15-yr timescale (Deser and Blackmon 1993).

In the present paper we study the role of the ocean in low-frequency climate variability by comparing several 1000-yr simulations: 1) a fully coupled run, 2) an atmosphere-only run with climatological SST and sea-ice conditions taken from run 1, and 3) a run in which the atmosphere is coupled to an 80-m slab mixed layer. The experimental setup strongly resembles Manabe and Stouffer (1996), and the present study is complementary to the latter.

Manabe and Stouffer compared the coupled run with a run in which the atmospheric component was forced with observed SSTs and sea-ice distribution. In the present study we derive the SST and sea-ice distribution from the climatology of the coupled run, in order to eliminate the effect of a time-mean different forcing of the atmospheric component. This enables us to compare the patterns of atmospheric variability (EOFs), their variance, and the (projection of) patterns of covariability found in the coupled run identified by a singular value decomposition (SVD). Decadal modes of covariability between atmosphere and ocean in ECBILT have been discussed before by Selten et al. (1999) and Haarsma et al. (2000). Here, we shortly discuss a decadal mode in the North Pacific. Also, we analyze time series of SAT and 800-hPa geopotential height (GEO) and intercompare the three different runs. We apply a statistical test to check whether the respective spectra fit an AR(1) process.

This paper is organized as follows. In section 2 we describe the atmospheric and oceanic model components and the series of numerical experiments that have been performed. In section 3 we describe the globally averaged spectra of the atmospheric variability in the various runs. In section 4 we focus on patterns of atmospheric variability and ocean–atmosphere covariability. In section 5 we present a discussion and our conclusions.

2. Experimental setup

a. Coupled model

The model used for the present study is “ECBILT,” a coupled climate model of intermediate complexity. It is a spectral T21 global three-level (800, 500, and 200 hPa) quasigeostrophic (QG) model with simple parameterizations for the diabatic processes (Haarsma et al. 1996). The dynamical component of the model was developed by Molteni (Marshall and Molteni 1993). The model is realistic in the sense that it contains the minimum amount of physics that is necessary to simulate the midlatitude planetary- and synoptic-scale circulations in the atmosphere as well as its variability on various timescales.

In order to improve the simulation of the Hadley circulation, as an extension to the QG equations, an estimate of the neglected ageostrophic terms in the vorticity and thermodynamic equations is included as a time and spatially varying forcing. The diabatic heating in the atmosphere is caused by the radiative heating, the release of latent heat and the exchange of sensible heat with the earth. The parameterizations of these processes are described in Haarsma et al. (1996). The model is, because of the QG approximation, two orders of magnitude faster than AGCMs. A serious limitation of ECBILT is that it cannot be used to study equatorial variability and consequently the interaction between the Tropics and the extratropics. For more details about the model we refer to Haarsma et al. (1996) and Opsteegh et al. (1998).

The OGCM is a primitive equation model, discretized on a geographical (locally Cartesian–Arakawa B) grid, with $5.625^\circ \times 5.625^\circ$ horizontal resolution and 12 layers in the vertical; these layers are spaced tens of meters near the surface, with increasing layer thickness toward the flat bottom at 4000-m depth. The OGCM is essentially a flat-bottom derivative of the Geophysical Fluid Dynamics Laboratory ocean model (Lenderink and Haarsma 1994). Sea ice is formed if the ocean temperature drops below -2°C . The effect of sea ice on the momentum transfer between atmosphere and ocean is neglected. The sea-ice model is based on the zero-layer model of Semtner (1976). The movement of sea ice is neglected. Various climatological fields can be found in Opsteegh et al. (1998), Selten et al. (1999), and Haarsma et al. (2000).

b. Experiments

Three 1000-yr runs were executed and analyzed.

- Coupled atmosphere–ocean: The ocean–atmosphere and sea-ice models were coupled without flux correction. The coupled model as a whole has been spun up for 5000 yr. The last 1000 yr of this spinup have been used to define the control climate.
- Atmosphere only: The daily mean ocean and sea-ice climatology of the coupled atmosphere–ocean run was used to force the atmosphere model.
- Coupled atmosphere–mixed layer: An 80-m layer of water that can store and give off heat, with a prescribed (daily mean climatological) horizontal heat transport replaced the ocean model in this experiment. This climatology is again obtained from the coupled run.

3. Globally averaged spectra for the midlatitudes

In this chapter we compare the averaged spectra of the atmospheric variability in midlatitudes between the three experiments described above. We focus on GEO and SAT. To obtain averaged spectra all spectral coefficients of the individual spectra in each grid box poleward of 22.5° and equatorward of 70° have been averaged in log scale.

a. Spectral characteristics

Locally, the atmospheric spectra of SAT and GEO are reddened due to coupling, as in, for instance, Bladé (1997). We loosely define redness as the increase of spectral variance with the period. For an AR(1) process the redness can be exactly determined, see for example Dommenges and Latif (2000, manuscript submitted to *J. Climate*, hereinafter DL). By doing so, we tacitly assume that the spectra can be described by an AR(1) process. Although this is not the case for all spectra discussed here, the difference between the average low-frequency variability level of these spectra and their red noise fits is small. For the present discussion, in which we try to understand the influence of the lower boundary on the low-frequency variance of SAT, these deviations are not relevant. Further below we will discuss more fully the implications of deviations from a red noise fit.

The integrated variance of 500-hPa geopotential height poleward of 20°N in Bladé’s mixed layer run was enhanced by 5%–20% when compared with the control run. The enhancement was 20% for 300-day averages, as compared with 5% for 30-day averages. Here, we consider longer timescales and near-globally averaged spectra for yearly averages. For timescales shorter than 5 yr coupling enhances the averaged variance of GEO up to 5% (Fig. 1). For timescales longer than 5 yr the enhancement increases to 15%. Differences between the coupled and mixed layer run are marginal. The increase

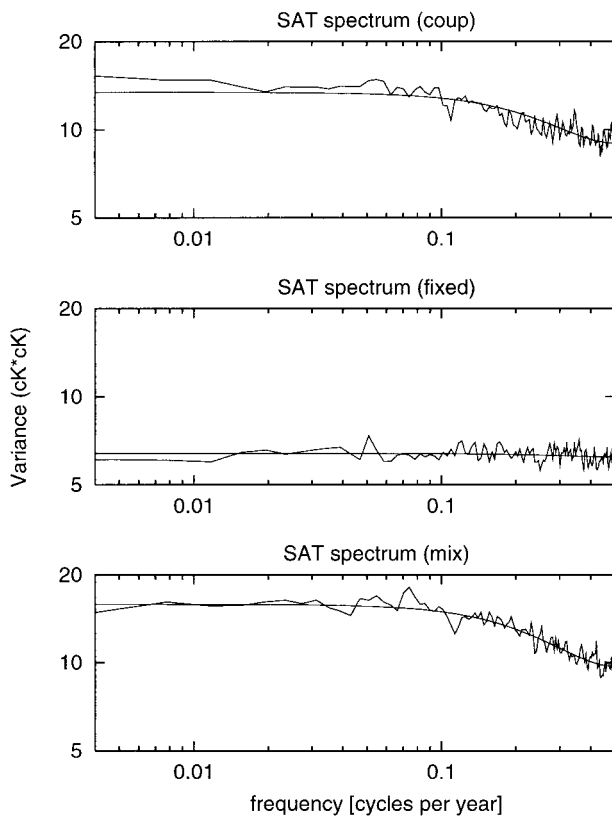


FIG. 2. Globally averaged spectra of yearly averaged SAT (cK^2) for the midlatitudes.

of enhancement of the variability with timescale due to coupling implies that coupling reddens the GEO spectra. Above ocean points, the increases of the GEO variance is somewhat larger than above land points (16% vs 13%). This extra enhancement is probably due to the adjustment of the oceanic mixed layer to the overlying atmospheric perturbations. The enhancement of GEO variability due to coupling is weaker than in Bladé's study. This enhancement is indirect, induced by the enhancement of SAT variability. The enhancement of SAT variability compares well to Bladé's results. The dynamical coupling between SAT and GEO is apparently different for the two models. Apart from the QG assumptions and simplified physics, the most likely explanation for this difference seems the lower vertical resolution of the present model.

The integrated variance of the temperature at 850-hPa geopotential height was enhanced by coupling with 5% for 30-day averages, 30% for 300-day averages in Bladé (1997). Here, for timescales shorter than 5 yr coupling enhances the globally averaged variance of SAT up to 25% (Fig. 2), coupling to a slab mixed layer yields an enhancement of 35%. For timescales longer than 5 yr the differences become even larger. In the coupled run the SAT variability is increased with 55%, in the mixed layer run with 90%. In the mixed layer

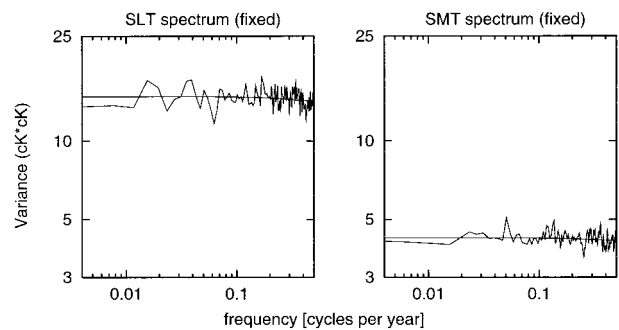


FIG. 3. Globally averaged spectra for the midlatitudes of SAT above land (SLT) and ocean (SMT) for the atmosphere-only run.

run SAT and SST are strongly coupled. Variability in heat fluxes drops to zero for timescales larger than 50 yr and the damping is weak on these timescales. With a prescribed heat transport the slab mixed layer does not contain dynamics of its own and SST is slaved to SAT. In the coupled run, ocean dynamics impedes this strong coupling. Both advection and upwelling generate SST patterns that do not match with the dominant SAT patterns that are the primary modes of atmospheric internal variability. As a result, both SAT and SST variability are damped in comparison with the mixed layer run, especially at the longer timescales and the spectrum of heat flux variability is less blue. So, not only the level of SAT variability but also the reddening of the SAT spectrum is overestimated in the mixed layer run. A simple coupled model is analyzed in the next section to shed more light on this.

b. A simple coupled model

To test the assumptions put forward above and to elucidate the role of ocean advection in reducing the variability of SAT and SST, we consider a simple coupled model of the ocean-atmosphere heat budget. The simple model will contain the essential physics that influence temperature spectra in ECBILT. We will not a priori derive the model to predict the spectra that follow from the various numerical experiments. Instead, we use the results from the numerical experiments to construct a simplified model that fits the associated low-frequency variability levels. These fits allow us to quantify terms in the respective heat budgets and to interpret how the ocean acts to damp SAT variability.

1) MODEL EQUATIONS

We consider datasets of yearly averaged temperature. We define temperature anomalies with respect to a 1000-yr average. We define T_{al} as the SAT anomaly above land (SLT), T_{ao} as the SAT anomaly above the ocean (SMT), and T_{oc} as the SST anomaly. We follow the approach of Hasselmann (1976) and assume that the atmospheric temperature contains a stochastic forcing

term ϵ . The equations for the three (anomalous) temperature variables become (see also Saravanan and McWilliams 1998)

$$(\partial_t + \alpha + \mu + \nu_a)T_{ao} = \mu T_{oc} + \epsilon \quad (1)$$

$$(\partial_t + \alpha + \nu_a)T_{al} = \epsilon \quad (2)$$

$$(\partial_t + \lambda + \nu_o)T_{oc} = \lambda T_{ao}, \quad (3)$$

where μ represents the damping of SAT anomalies by heat exchange with the ocean, λ the damping of SST anomalies by heat exchange with the atmosphere, and α is an atmospheric damping coefficient due to radiative heat loss to space. Taking the coupling coefficient for the air–sea heat flux to be $20 \text{ W m}^{-2} \text{ K}^{-1}$ and the sensitivity of the upward atmospheric longwave radiation to be $3 \text{ W m}^{-2} \text{ K}^{-1}$, $(\mu)^{-1}$ is about 5 days; $(\alpha)^{-1}$ is about 40 days. We have written $\mathbf{U} \cdot \nabla T$ as νT , where $(\nu)^{-1}$ is an effective damping timescale due to advection. Locally, the effect of advection cannot be described as a damping term. Advection can both create and destroy anomalies. Spatially and time averaged, however, the effect of advection on atmospheric low-frequency fluctuations is dominated by the diffusive effects of transient eddies on quasi-stationary waves. This results in a typical damping timescale for low-frequency fluctuations of the order of 10 days, see Saravanan and McWilliams (1998). For the time being we assume that a similar damping effect occurs in the ocean.

Obviously, the treatment of advective damping in Eqs. (1), (2), and (3), especially with its lack of land–sea air temperature coupling is too crude to fit the full model results. Nevertheless, the simple model will be used to fit the low-frequency variability level. Neglecting advection and putting ν to zero, the variance spectra of the response $G_{al}(\omega)$ and the input $\mathcal{E}(\omega)$ that are related in the time domain by Eq. (2) are related in corresponding frequency intervals through

$$G_{al}(\omega) = \frac{\mathcal{E}(0)}{(\omega^2 + \alpha^2)}. \quad (4)$$

This response spectrum levels off to

$$G_{al}(0) = \frac{\mathcal{E}(0)}{\alpha^2}. \quad (5)$$

It is easy to show that also $G_{ao}(0)$ and $G_{oc}(0)$ attain the same value.

When atmospheric advection is included the atmospheric damping increases and the response decreases:

$$G_{al}(0) = \frac{\mathcal{E}(0)}{(\alpha + \nu_a)^2}. \quad (6)$$

The value of ν_a can be estimated from the uncoupled experiment. In this experiment the term μT_{oc} drops from the rhs of Eq. (1). Then,

$$G_{ao}(0) = \frac{\mathcal{E}(0)}{(\mu + \alpha + \nu_a)^2}. \quad (7)$$

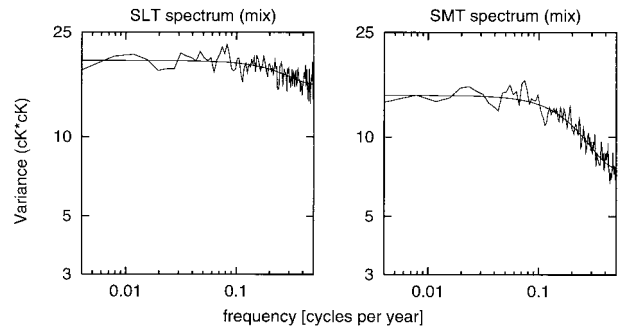


FIG. 4. Globally averaged spectra for the midlatitudes of SAT above land (SLT) and ocean (SMT) for the slab mixed layer run.

From the ratio of $G_{ao}(0)$ to $G_{al}(0)$ ν_a is estimated. This number is 0.36 (Fig. 3). Then, $\nu_a = 1.5\mu$, implying an atmospheric damping timescale of 3.5 days, which is rather short. In the full model, land–sea air temperature are partially coupled acting to decrease the ratio of the respective low-frequency responses. As a result, the effective atmospheric damping timescale is underestimated. We conclude two things from Fig. 3: 1) atmospheric advection strongly reduces the low-frequency response; 2) in the absence of coupling between SAT and SST anomalies, heat loss to the ocean strongly damps SAT variability above sea.

When the atmosphere is coupled to a slab mixed layer, SMT and SST anomalies become completely coupled at low frequencies. As a result, $G_{oc}(0)$ and $G_{ao}(0)$ become equal to $G_{al}(0)$; Eq. (6). From Fig. 4, we see, however, that the ratio between $G_{ao}(0)$ and $G_{al}(0)$ is 0.75. Also, an experiment in which the effect of radiative heating at the interface on temperature anomalies was neglected yielded a ratio significantly below 1: 0.8. This suggests that damping due to atmospheric advection is larger above the ocean than above land. This may result from the wind speed and its variability being larger above the ocean. Also, the spatial scales of SAT anomalies above the ocean could be smaller. That this is indeed the main factor in causing different spectra is motivated by the different response levels in the Northern and Southern Hemispheres (not shown). Above the ocean the low-frequency response attains the same values in both hemispheres where the ocean basins have equal size, but the response above land is much smaller in the Southern Hemisphere where the landmasses are small.

At the western side of the continents a maritime climate prevails and SAT variability is dominated by intrusions from sea. There, the SAT variability should be similar to that above the ocean. Further inland continental-size SAT anomalies may develop. In the Northern Hemisphere midlatitudes the largest scales are associated with the Eurasian continent. Especially there, we expect the low-frequency SAT variability above land to be larger than the SAT variability above the ocean. In the Southern Hemisphere midlatitudes the landmasses

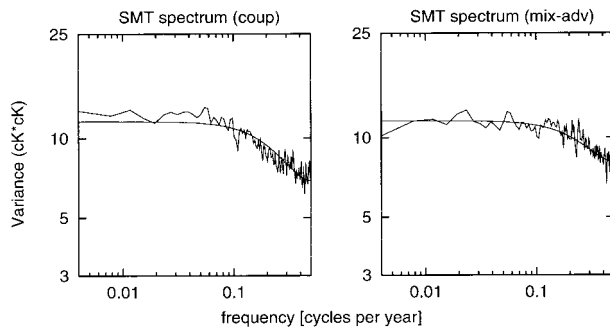


FIG. 5. Globally averaged spectra for the midlatitudes of SAT above the ocean (SMT) for the coupled run and the mixed layer run including advection.

are small and influenced by either marine SAT anomalies, or at the eastern halves by smaller-scale continental-size anomalies. Comparing Figs. 4a and 3a we also see that the spectral levels of SLT at low frequencies are not equal although in both cases Eq. (6) applies. The spectrum above land will be affected by advection of marine air and in the atmosphere only run $G_{ao}(0)$ is much lower than in the slab mixed layer run.

In the fully coupled run we must also take oceanic advection into account. When ocean advection induces SST variability that does not match the internal SAT variability, ocean advection will act to damp temperature variability. It can be found that the response spectra G_{oc} and G_{ao} level off to

$$G_{ao}(0) = G_{oc}(0) = \frac{\mathcal{E}(0)}{[v_a + v_o(\mu + v_a)/\lambda]^2}. \quad (8)$$

We assume that v_o/v_a roughly scales with U_o/U_a . Taking a typical ocean velocity of 0.01 m s^{-1} and a typical wind speed of 5.0 m s^{-1} , $(\mu + v_a)/\lambda(v_o/v_a)$ becomes 0.1. When temperature variability associated with atmospheric and oceanic motion is uncorrelated, $G_{oc}(0)$ and $G_{ao}(0)$ drop with 20% due to ocean advection [cf. Eqs. (7) and (8)].

Comparing the coupled run with the slab mixed layer run, we observe that the response spectrum of T_{ao} at low frequencies drops with 25% (Figs. 4b and 5a). Now, the coupled run compared to the slab mixed layer run not only includes advection, but also diffusion, convective mixing, a spatially varying mixed layer depth, and dynamically induced variations in the local mixed layer depth. To isolate the role of ocean advection we repeated the mixed layer run, but now the SST anomalies are advected with the mean flow derived from the coupled run. In this experiment $G_{ao}(0)$ nearly equals that in the fully coupled experiment (Fig. 5). So we conclude that ocean advection is the main cause for the different spectra between a slab mixed layer and fully coupled run.

These results corroborate the findings of Manabe and Stouffer (1996). They found that the spectral density above continents is larger than above the ocean, partic-

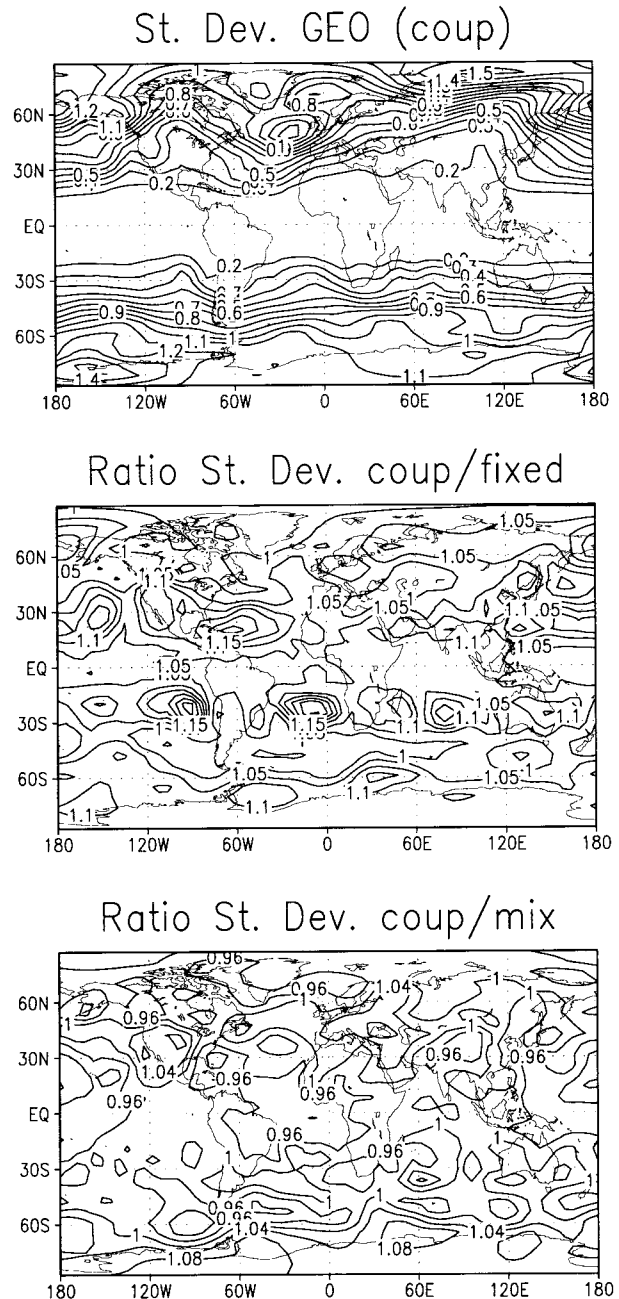


FIG. 6. Global pattern of yearly averaged variability of (a) GEO (dam^2) and below the ratio of local GEO variability of the coupled run over (b) the fixed SST and (c) slab mixed layer runs.

ularly at high frequencies, where the thermal inertia of the ocean reduces the magnitude of the anomalies. Although the ocean adjusts to SAT fluctuations on time-scales longer than the decorrelation timescale of the mixed layer (4 months or so), this adjustment is never complete and the ocean remains a sink for SAT fluctuations, but more so for the higher frequencies than for the lower frequencies, and more so when ocean advection becomes important.

2) AR(1) PROCESSES

So far we assumed that all spectra fit to AR(1) processes. We deliberately omitted the 95% confidence intervals when showing these spectra because it is far from trivial to estimate these in the present case. The reason is, that these spectra are not simply related to a time series of an observable, but obtained from averaging the spectral coefficients of each midlatitudinal grid box. As time series between different grid boxes will be correlated and the correlation coefficients feature complex spatial dependencies, confidence intervals are not easily established. For that reason we discarded the idea of testing the averaged spectra, but we have tested each individual spectrum whether it fits to an AR(1) spectrum. Similar tests have been performed on spectra of SST by Reynolds (1978) and DL. Reynolds assumed a Gaussian distribution for the quantity

$$E = \sum_{i=2}^N [\log(e_i) - \log(t_i)]^2 \quad (9)$$

with e_i the spectral coefficients of the data; t_i the spectral coefficients of the hypothesized spectrum; and N the number of channels, and tested whether it exceeded a critical value. In their study, DL compared E with 1000 realizations of

$$R = \sum_{i=2}^N [\log(r_i) - \log(t_i)]^2 \quad (10)$$

with r_i the spectral coefficients of a single realization of an AR(1) time series of the same length as the data and t_i the true spectral coefficients of the AR(1) process.

Both Reynolds (1978) and DL found that ocean dynamics affect the SST spectra, becoming significantly different from an AR(1) process. Dommenges and Latif argued that this is due to heat exchange of the mixed layer with the sub-mixed layer ocean that leads to a slower but longer increase of SST variance from shorter to longer time periods, characterized by increased variance at the seasonal and decadal timescales. But the mixed layer dynamics cannot explain the total impact of ocean dynamics on the SST spectra. Their Fig. 8 shows that the confidence levels for rejecting the hypothesis that the SST spectra agree with an AR(1) process are higher for both observations and the fully coupled models than when a dynamical mixed layer is used, which on its turn shows higher confidence levels than in case of a fixed, slab mixed layer.

For all averaged spectra shown here, we tested for each grid box whether E falls within the 95% lowest numbers of 1000 realizations of R . To make a statement on whether all individual spectra fit the AR(1) process, we consecutively tested the hypothesis that in no more than 5% of the grid boxes the null hypothesis is rejected. The confidence level to reject this hypothesis was also chosen to be 95%. For the present model all averaged spectra agree with an AR(1) process, apart from SMT

in the coupled run (Fig. 5a). This result is in agreement with DL. Apparently, only the coupled run induces the ocean dynamics that can make the SST spectra deviate from an AR(1) process, and due to the coupling, the SMT spectra. When the role of ocean dynamics is strong enough to cause substantial deviations from an AR(1) process in the SMT spectra in a larger number of grid boxes, then one would expect through coupling of land-sea air temperature the SLT spectra to deviate from an AR(1) process. In the present model, however, that is not the case.

The role of ocean dynamics in the present model seems weaker than it is in the coupled models discussed in DL. In most grid boxes the hypothesis that the SMT spectrum fits an AR(1) process is not rejected. The ocean model used here features rather coarse resolution and weak currents. Also, in the LSG model in DL, more points fit the AR(1) process than in both the higher-resolution OPYC model and the observations. The HOPE model does not seem to benefit from the higher resolution in this respect. Since mixed layer dynamics do not explain all the deviations of the SST spectra from an AR(1) process, one may expect that in models in which higher resolution and weaker friction allows for higher Reynolds numbers, the role of ocean currents in affecting the SST spectra and subsequently the spectra of SMT increases.

We also tested whether the spectra deviate from white noise. For GEO this is nowhere the case. Apart from the atmosphere-only run, in all runs the spectra of SMT deviate from white noise. The spectra of SLT only do so in the mixed layer runs. As in those runs the spectra for SMT are much redder than they are in the coupled, or atmosphere-only run, through coupling of land-sea air temperature the spectra of SLT also become more red in the mixed layer runs. In the atmosphere-only run the selective damping at higher frequencies by the ocean does not apply, and all spectra remain white.

4. Patterns of variability

a. Standard deviation

Spatial distributions of yearly averaged variability in GEO and SAT for the coupled run are presented in Figs. 6a and 7a. They show a generally zonally symmetric pattern, with higher values at higher latitudes. This and the overall amplitude are consistent with observations and the results of Manabe and Stouffer (1996) for SAT and Bladé (1997) for GEO. In the present model this tendency is exaggerated as values in the tropical regions are unrealistically low in ECBILT, due to the QG scaling. Deviations from the zonal symmetry in the variability in SAT and GEO are related to land-sea contrasts. SAT variability is higher above land as it is damped by heat exchange with the ocean, GEO variability is higher above the ocean where the major storm tracks are.

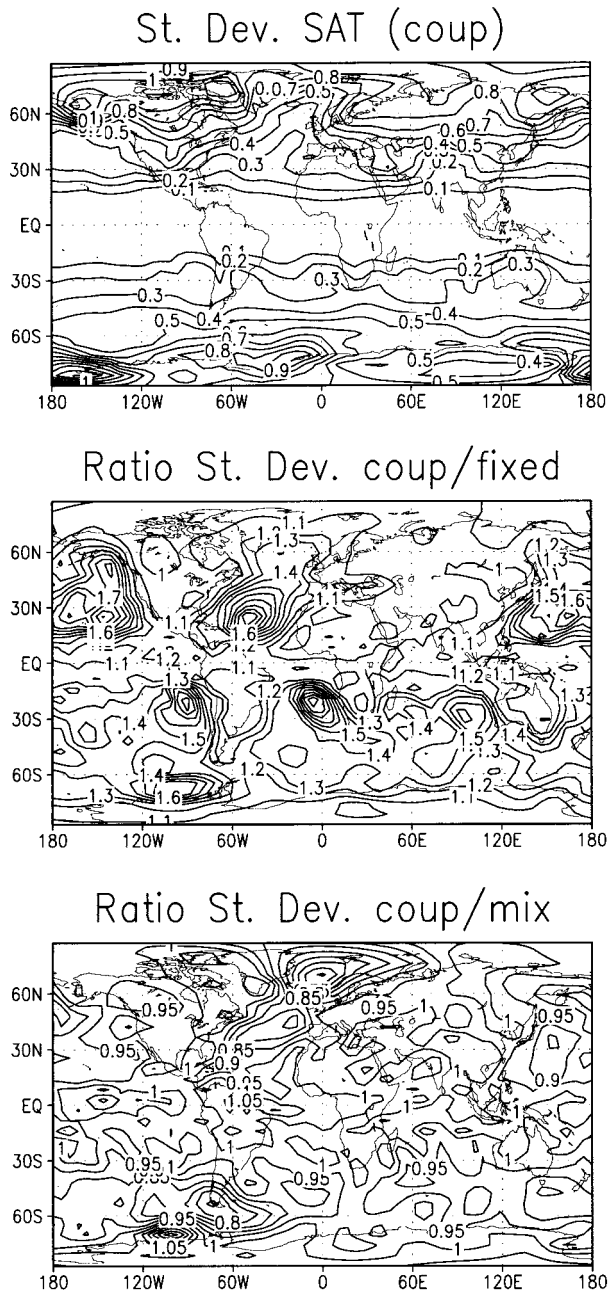


FIG. 7. Global pattern of yearly averaged variability of (a) SAT (K^2) and below the ratio of local SAT variability of the coupled run over (b) the fixed SST and (c) slab mixed layer runs.

As compared with the fixed ocean run, coupling somewhat enhances variability in GEO (Fig. 6b, in general between 0% and 15%), with maxima at the subtropical ocean between 20° and 30° . A weak impact of coupling on the variability in geopotential height was also found in Bladé (1997). In that study maximal enhancement was located somewhat farther poleward (between 30° and 50°). This may (partly) be explained by the jet stream being displaced equatorward in our model

(Opsteegh et al. 1998). SAT shows maximal enhancement at the same locations but up to 80% (Fig. 7b). This effect is robust in many previous studies. Coupling enhances the variance of SAT, up to a doubling above the tropical ocean (Manabe and Stouffer 1996; Barsugli and Battisti 1998). Outside the Tropics the enhancement due to coupling compares well with the more comprehensive model of Manabe and Stouffer (1996). Barsugli (1995) explained this by an adjustment of the oceanic mixed layer to SAT anomalies. Consequently, the SST variability in the ocean attenuates the damping of SAT anomalies compared to prescribed SSTs and enhances their persistence by reducing the negative feedback of the air–sea heat flux. This role of coupling in reducing the heat flux variability and increasing the SAT variability has been confirmed by, for example, Bhatt et al. (1998).

In agreement with the characteristics of the averaged spectra, coupling to a slab mixed layer in stead of a dynamically active ocean slightly overestimates the variability in SAT and GEO (Figs. 6c and 7c). The attenuation of the damping of SAT anomalies by the adjustment of the oceanic mixed layer temperature to these anomalies is stronger when ocean dynamics is absent, that is a slab mixed layer is more “slaved” to the atmosphere than a dynamically active ocean. As a result, SAT variability is enhanced up to 10% by coupling to a mixed layer ocean; GEO variability is enhanced up to 5%. The impact of ocean dynamics on GEO is indirect. As SAT and sea level pressure (GEO in our case) are dynamically coupled a reduction in SAT variability induces a decrease in GEO variability.

b. EOF analysis

The 20 leading EOF patterns for each variable for various basin-scale regions, together with their principal components (PCs), formed the basic data for our analysis. The first two dominant EOF patterns typically explain 30%–10% of the variability in the basin-scale areas and 10%–5% in the global and hemispheric domains. In the coupled run the leading EOFs for GEO and SAT are similar to EOFs of the observed variability (Wallace et al. 1990) in a number of instances that we checked: for instance, comparing the SLP EOFs in the North Pacific and North Atlantic areas calculated by Cayan (1992) with EOFs of GEO from our experiments (Fig. 8), we find that, although the patterns are not identical, the origin and character of the variability indicated by these EOF patterns are clearly the same and reflect similar physical mechanisms. The two dominant EOFs in the North Atlantic and North Pacific are associated with the midlatitude westerlies (which are weaker, more diffuse, and displaced southward relative to observations, see Opsteegh et al. 1998). A north–south dipole in SLP (observed EOF 2 in the North Pacific and observed EOF 1 in the North Atlantic) indicates strengthening or weakening of the pressure structure associated

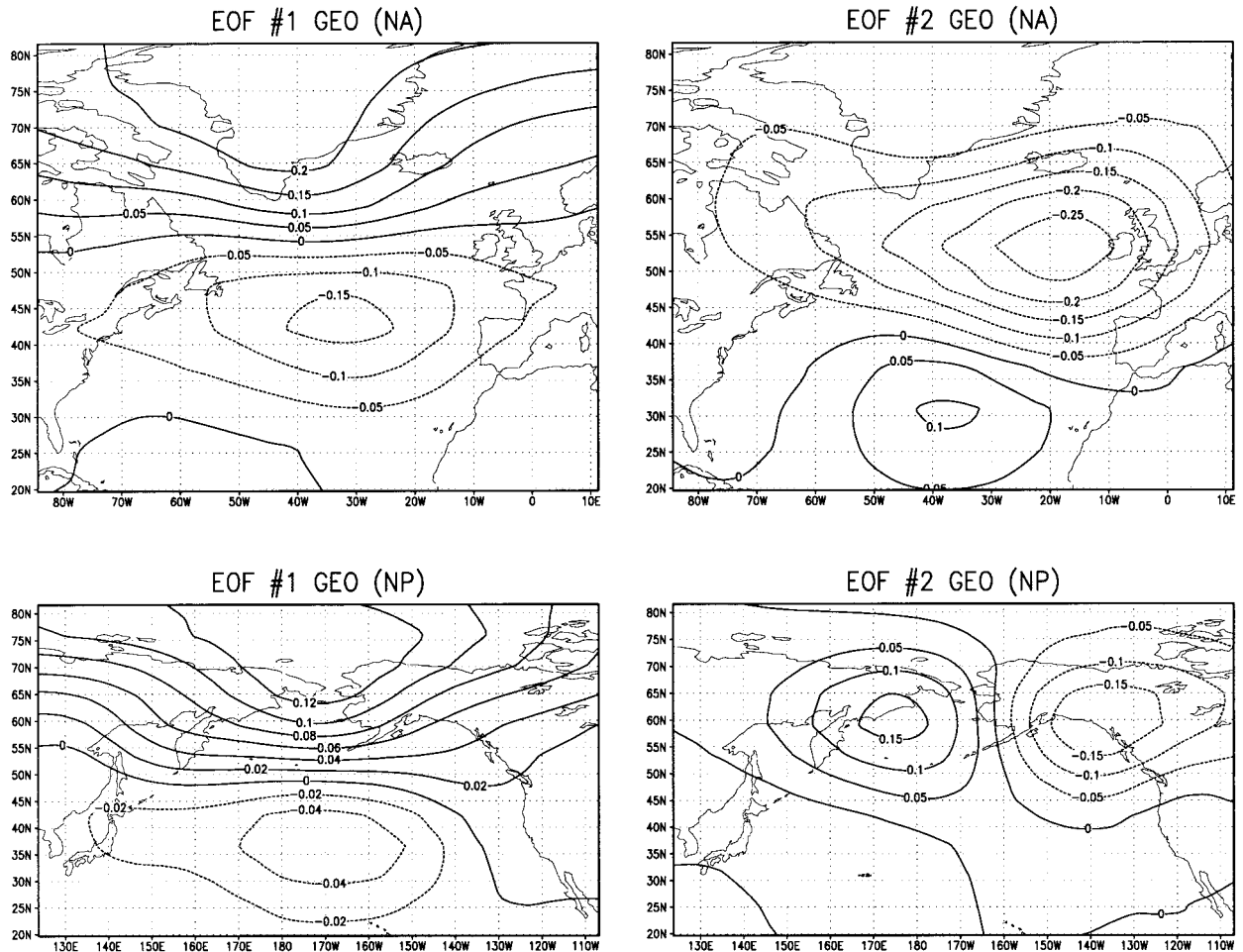


FIG. 8. First two EOFs of winter mean GEO anomalies for the North Atlantic and North Pacific regions.

with the jet and thus an intensification or weakening of jet and westerlies. A monopole structure at the location of the axis of the jet indicates meridional movement of jet and westerlies.

The leading EOFs for GEO and SAT are very similar between the three experiments; for all experiments, the same set of six regional patterns (per variable) describes about 75% of the variance in each region. This confirms the previous findings of Delworth (1996), Bladé (1997), and Bhatt et al. (1998). Also after applying a 5-yr running mean on the data before analyzing, the dominant patterns of atmospheric variability are not affected by coupling. In the present study we find that there is no significant difference in explained variance for the leading EOFs between the three experiments. This contradicts the findings of Delworth (1996), Bladé (1997), and Bhatt et al. (1998). In those studies the relative importance of the leading EOF patterns was sensitive to coupling and whether coupling was achieved with a slab mixed layer or a dynamically active ocean. Differences between our analysis and the aforementioned ones are that we emphasize longer timescales.

On the other hand, the notion that the spatial patterns associated with the response to SST anomalies closely resembles the the dominant patterns of internal variability implies that the internal variability strongly influences the response to SST anomalies, which is typical for nonlinear dynamical systems that exhibit regimelike behavior (Palmer 1999; Venzke et al. 1999). In such a case, one would expect that the probability density distribution of the associated PC time series would change due to coupling. In all three experiments, however, the frequency distributions of the PC time series do not deviate significantly from Gaussian distributions. Such a Gaussian frequency distribution of the leading EOFs is not uncommon in typical low-resolution climate models (Rowell 1998), although the observations show signs of multimodal frequency distributions (Corti et al. 1999). A plausible explanation for the lack of regime behavior in the present, and other, coupled OAGCMs is the underestimation of (smaller scale) transients in those models. Also, it could be that multimodality is weaker, or even absent, at larger timescales. For instance, Tett et al. (1997) found evidence for multimodal

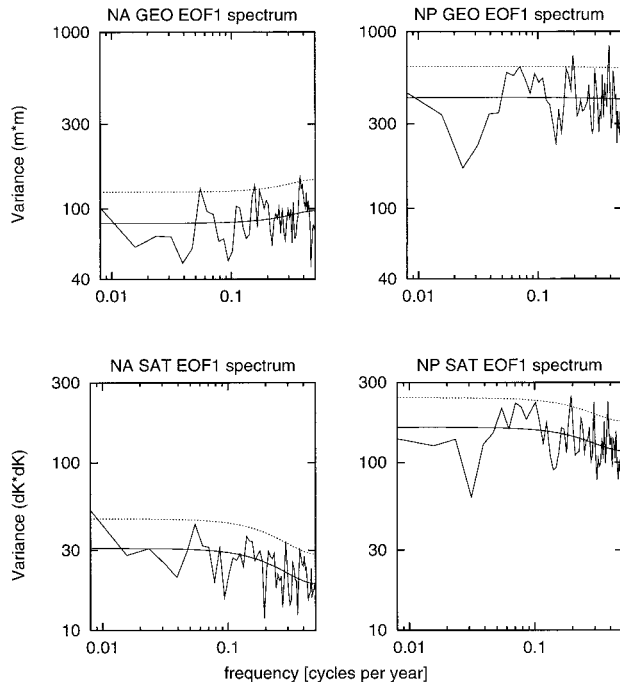


FIG. 9. Spectra of the PCs of dominant GEO EOFs (m^2) and SAT EOFs (dK^2) for the North Atlantic and North Pacific.

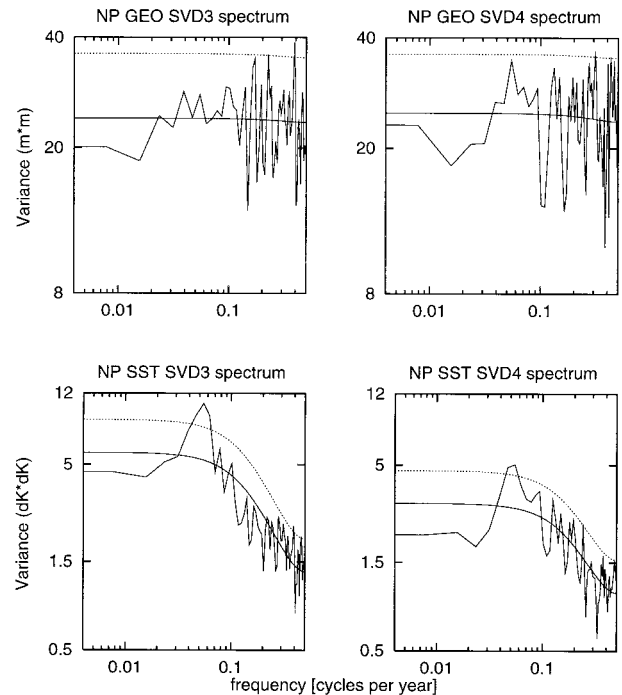


FIG. 10. Spectra of the PCs of the third and fourth SVD mode of winter mean SST anomalies (dK^2) and GEO anomalies (m^2) for the North Pacific.

dality in their model, but not that regimes persist on annual or greater timescales.

The temporal behavior of the EOFs was further investigated by Fourier analysis of the PC time series. In general, the spectrum is in agreement with the fitted AR(1) process (Fig. 9), the GEO spectra do not deviate from white noise. Occasional peaks that rise above the 95% confidence interval are spurious, because they do not show up consistently when the analysis is repeated for the first and second half of the data. Therefore, our model does not support the results of James and James (1992) that the atmosphere itself can generate low-frequency variability with a preferred timescale.

c. Coupled modes

Here we analyze whether the coupling strategy (slab mixed layer vs dynamically active ocean) affects the principal modes of covariability and whether the spectra of these modes are changed. To this end we apply an SVD analysis of SMT and SST and of GEO and SST (truncated to the 20 leading EOFs), following Bretherton et al. (1992).

We find in most regions that a few dominant SVD patterns tend to show temporal correlation coefficients of 0.6–0.7 and we discard SVD pairs with correlation coefficients less than 0.6. Often (but not always) the SST pattern and spectrum in an SST–SAT pair are very similar to that of the SST–GEO SVD pair of the same ranking, indicating that both SVD pairs are related to the same physical structure. Typical leading SVD pat-

terns and coefficient time series that we find are similar to the leading EOF patterns and PCs.

Spectral features above the 95% confidence interval are taken to indicate a “coupled mode” if the spectral peak shows up in both (or all four) SVD coefficient time series and in both halves of each 1000-yr run. These significant modes typically project strongly on one or two high-ranking EOF patterns and explain between 15% and 30% of the squared covariance. We scanned all extratropical basins for the existence of coupled modes. The coupled model features three such coupled modes.

In the North Atlantic, the second SVD mode shows a significant peak in the 14–16-yr period range. The GEO pattern is ECBILT’s equivalent of the North Atlantic Oscillation (NAO) pattern. This SVD mode was analyzed in Selten et al. (1999). Another region where significant decadal timescale covariability in atmosphere and ocean arises is the Southern Ocean. SVD patterns show characteristics of a traveling wave similar to the Antarctic Circumpolar Wave (ACW). This mode was investigated by Haarsma et al. (2000).

SVD analysis of the North Pacific covariability between SST and SMT or GEO show decadal timescale variability in the range of 18–20 yr, in the form of spectral peaks that are significantly different from the background red noise in the time series of the SST (and SMT) patterns of SVD 3 and 4 (Fig. 10). Both SVD pairs consist of a zonally oriented chain of alternating positive and negative anomalies (Fig. 11). The physical

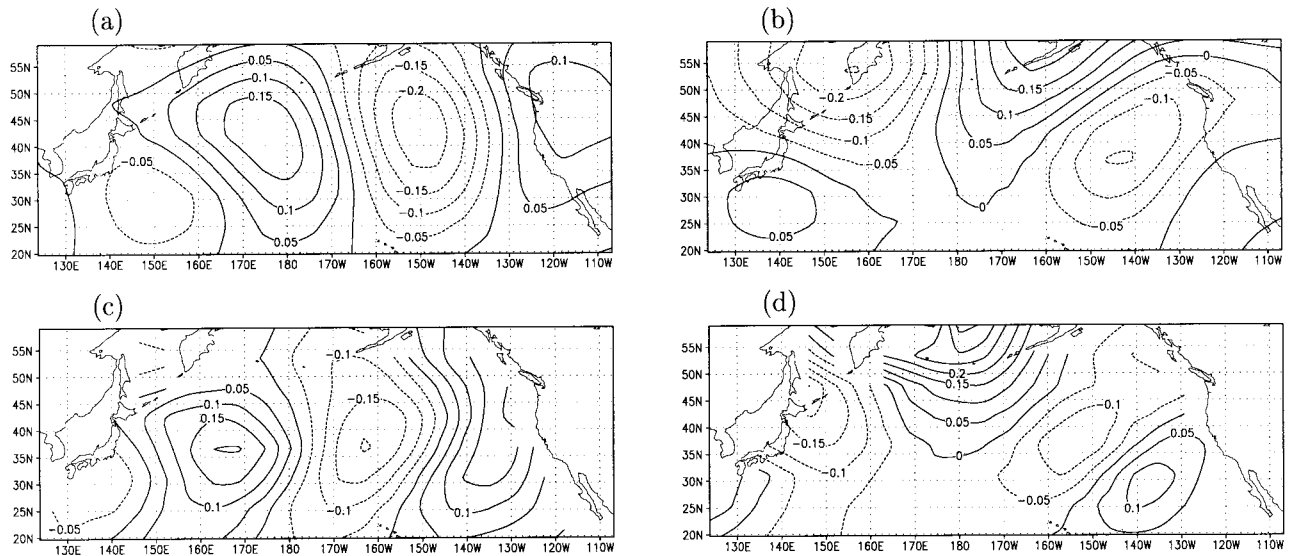


FIG. 11. Third and fourth SVD mode of winter mean (c), (d) SST anomalies (K) and (a), (b) GEO anomalies (dam) for the North Pacific.

connection between the GEO anomalies and the SST anomalies are consistent with the atmospheric anomalies creating the SST anomalies; anomalous northerly (southerly) winds overly anomalous cold (warm) SSTs. Although the GEO patterns of both SVDs tend to be in quadrature spatially, no west–east propagation can be detected in the atmosphere. On the other hand, clear propagation of temperature and salinity anomalies is visible in the ocean, especially in the subsurface (80–300 m). In about 20 yr, alternating positive and negative anomalies travel the entire Pacific Ocean from Japan to California where they are dissipated by mixing.

Although a complete analysis of this mode is beyond the scope of the present paper, we did analyze two sensitivity integrations to shed some more light on the physical mechanism. In one integration, the atmosphere did not “see” the actual SSTs, but the SSTs of one particular year of the coupled integration. The ocean was forced with the varying winds and temperatures of the atmosphere. We refer to this integration as a one-sided coupled integration. In this run the same SVD modes were found, the SST variability was reduced, and significant peaks in the spectra of the SST variations were no longer found. However, in the subsurface the propagating SST and salinity anomalies were still there with the same timescale. As for the North Atlantic decadal mode (Selten et al. 1999), the atmospheric response is not required for the generation of the subsurface oscillation, but is needed to express the oscillation in ocean surface variables by reducing the damping of SST anomalies. In the other sensitivity integration, the ocean velocities were fixed to the climatological annual cycle of the coupled integration. If in this integration, the subsurface oscillation is still present, the advective resonance hypothesis forwarded by Saravanan and McWilliams (1998) might explain the oscillation. However, the sub-

surface oscillation disappeared in this run, which leads us to conclude that anomalous ocean currents in response to density changes and/or changes in the wind stress play a crucial role in its creation.

For all three coupled modes significant spectral peaks only occur in the coupled run. The slab mixed layer run shows similar patterns of covariability, but no spectral peaks are present. Covariabilities, however, are higher, reflecting the relative “ease” by which the atmosphere pattern is imprinted on the slab mixed layer. The squared covariance of the associated (leading) SST–EOFs is also somewhat larger in the mixed layer experiment. Also, when the patterns of the coupled mode are projected on the data of the mixed layer or fixed SST run, there are no spectral peaks. Comparing SVD patterns between the fully coupled run, the slab mixed layer run and a one-way coupled run showed that coupling hardly affects the modes of covariability.

5. Discussion and conclusions

a. Discussion

Comparing the results from this study and previous studies with the present model (Selten et al. 1999) suggests the following mechanisms for interannual midlatitude atmosphere–ocean variability to be active in the present model.

The dominant patterns of internal atmospheric variability are not affected by coupling. The ocean does not imprint specific response patterns to the atmosphere. Dominant patterns of SST variability are coupled to dominant patterns of SAT that are inherent to the internal atmospheric variability. Ocean wave dynamics and mean flow advection induce patterns of interannual/decadal variability in the subsurface. There, together

with the signal of subducted (forced) SST variability, they may give rise to oscillations. Such an oscillation can be decomposed in a forced and advective phase (Selten et al. 1999), which are in quadrature and are associated with, respectively, a pattern of subducted SST variability and a pattern induced by ocean dynamics. Ocean dynamics may feed back on the pattern of subducted SST variability and cause a phase reversal, leading to a preferred timescale. In Selten et al. (1999) anomalous convection due to salinity anomalies provided this feedback.

The advective phase of a subsurface oscillation is strongly damped in SST as it does not match the dominant patterns of internal atmospheric SAT variability. There arises no counterpart of the subsurface oscillation in SST. The forced phase of the subsurface oscillation is coupled to the dominant patterns of SST by reentrainment and it *does* match the dominant patterns of SAT variability. As a result, the preferred timescale arises in the associated SST and SAT pattern as a standing oscillation. An alternative mechanism for interannual variability in SAT and SST is that ocean advection may carry away the forced SST signal and a preferred timescale arises that is the ratio of the length scale of the SAT pattern and the ocean advection velocity (Saravanan and McWilliams 1998). This mechanism operates in the Southern Ocean in case of the ACW (Haarsma et al. 2000).

We found no compelling evidence of preferred timescales arising in GEO. It might be that a more sophisticated atmospheric model with higher vertical resolution is needed to assess in which conditions a preferred timescale in a specific SAT pattern can be associated with a preferred timescale in certain SLP and GEO patterns and in which conditions not. A lack of horizontal resolution in the ocean model may cause an underestimation of the role of ocean dynamics in inducing SST variability, due to weaker gradients, too small velocities, and a too strong horizontal diffusion. Hall and Manabe (1997) and Goodman and Marshall (1999) suggest that at some places, and on decadal timescales, ocean advection may become as important for the SST variability as surface heat exchange. But the finding that the advective phase of a subsurface oscillation is always more strongly damped at the surface than the forced phase will also hold for higher-resolution models, and it does not seem likely that the ocean is able to imprint an advective phase pattern to the atmosphere with an amplitude that is comparable to the dominant patterns of internal variability.

b. Summary and conclusions

Three 1000-yr simulations of the global atmospheric circulation with an atmospheric GCM of intermediate complexity coupled to, respectively, a fixed (prescribed) ocean surface, an 80-m slab mixed layer model, and an ocean GCM are described and analyzed. In agreement

with previous studies both reddening of the spectrum and SAT variability are highest in the slab mixed layer experiment. Damping of SAT variations is reduced by coupling, especially at longer timescales. This reduction is strongly overestimated in the slab mixed layer run because the SST anomalies are coupled too strong to SAT anomalies due to a lack of ocean dynamics. A one-dimensional stochastic model is developed to explain the damping of SAT anomalies. It appears that ocean advection, creating patterns of SST variability that do not match the preferred modes of SAT variability, is the main cause for damping SAT anomalies above the ocean. In the coupled run ocean dynamics induce systematic deviations from the fitted AR(1) process in the SAT spectra above sea.

The global patterns of the standard deviation for the yearly averaged SAT and GEO show that coupling slightly enhances the GEO variability and the SAT variability somewhat more, up to 80%. EOF analysis of the variability in midlatitude regions shows that the leading patterns (which are essentially the same in all three experiments) are similar to observations (allowing for the shortcomings of the models), implying underlying physical mechanism. The dominant patterns of lower atmospheric variability are not affected at all by coupling. Comparing the spectra of the PCs in the EOF analyses with spectra from an AR(1) process we conclude that the general characteristics of midlatitude low-frequency atmospheric variability can be described by such a stochastic model. Significant spectral peaks are absent in all PC time series. These results corroborate earlier findings.

SVD analysis of the atmosphere–ocean covariability yields in most regions a few dominant patterns with temporal correlation coefficients of 0.6–0.7. Significant *modes* (with spectral features above the 95% confidence interval) typically project strongly on one or two high-ranking EOF patterns and explain between 15% and 30% of the squared covariance. Three modes are identified in the coupled experiment. In the North Atlantic a decadal mode is found resembling the NAO pattern. Also, the North Pacific shows decadal timescale variability. The covariability of SST and GEO in the Southern Ocean region shows a mode similar to the Antarctic Circumpolar Wave. In all cases projection of the patterns of the coupled run to the data of the mixed layer or fixed SST runs yields amplitude time series without spectral peaks.

In the current model two mechanisms for coupled variability at interannual timescales can be identified. One mechanism is the modification of forced SST patterns by ocean advection that introduces a preferred timescale determined by the ratio of the length scale of the SST pattern and the advective velocity (Saravanan and McWilliams 1998; Haarsma et al. 2000). The second mechanism is the coupling in the subsurface of a pattern associated with ocean dynamics to a pattern of subducted (forced) SST variability. Both patterns are in

quadrature and form together an oscillation (Selten et al. 1999). The resulting preferred timescale is imprinted upon the forced SST pattern by reentrainment, and subsequently upon the associated SAT pattern by air–sea interaction. Whereas in the subsurface a traveling mode can be identified, in SST and SAT mostly a standing oscillation is apparent.

Acknowledgments. Comments of one anonymous reviewer led to significant improvements in the manuscript. We like to thank Theo Opsteegh for providing useful comments.

REFERENCES

- Barsugli, J. J., 1995: Idealized models of intrinsic midlatitude atmosphere–ocean interaction. Ph.D. dissertation, University of Washington, 189 pp. [Available online at <http://www.cdc.noaa.gov/jjb/thesis.html>]
- , and D. S. Battisti, 1998: The basic effects of atmosphere–ocean thermal coupling on midlatitude variability. *J. Atmos. Sci.*, **55**, 477–493.
- Bhatt, U. S., M. A. Alexander, D. S. Battisti, D. D. Houghton, and L. M. Keller, 1998: Impact of an interactive North Atlantic Ocean on interannual midlatitude climate variability. *J. Climate*, **11**, 1615–1632.
- Bladé, I., 1997: The influence of midlatitude ocean–atmosphere coupling on the low-frequency variability of a GCM. Part I: No tropical SST forcing. *J. Climate*, **10**, 2087–2106.
- Bretherton, C. S., C. Smith, and J. M. Wallace, 1992: An intercomparison of methods for finding coupled patterns in climate data. *J. Climate*, **5**, 541–560.
- Cayan, D. R., 1992: Latent and sensible heat flux anomalies over the Northern Oceans: Driving the sea surface temperature. *J. Phys. Oceanogr.*, **22**, 859–881.
- Corti, S., F. Molteni, and T. N. Palmer, 1999: Signature of recent climate change in frequencies of natural atmospheric circulation regimes. *Nature*, **398**, 799–802.
- Delworth, T. L., 1996: North Atlantic interannual variability in a coupled ocean–atmosphere model. *J. Climate*, **9**, 2356–2375.
- , S. Manabe, and R. J. Stouffer, 1993: Interdecadal variations of the thermohaline circulation in a coupled ocean–atmosphere model. *J. Climate*, **6**, 1993–2011.
- Deser, C., and M. L. Blackmon, 1993: Surface climate variations over the North Atlantic Ocean during winter: 1900–1989. *J. Climate*, **6**, 1743–1753.
- Drijfhout, S. S., C. Heinze, M. Latif, and E. Maier-Reimer, 1996: Mean circulation and internal variability in an ocean primitive equation model. *J. Phys. Oceanogr.*, **26**, 559–580.
- Ferranti, L., F. Molteni, and T. N. Palmer, 1994: Impact of localized tropical and extratropical SST anomalies in ensembles of seasonal GCM integrations. *Quart. J. Roy. Meteor. Soc.*, **120**, 1613–1645.
- Frankignoul, C., and K. Hasselmann, 1977: Stochastic climate models. Part II: Application to sea-surface temperature anomalies and thermocline variability. *Tellus*, **29**, 289–305.
- , P. Müller, and E. Zorita, 1997: A simple model of the decadal response of the ocean to stochastic wind forcing. *J. Phys. Oceanogr.*, **27**, 1533–1546.
- Goodman, J., and J. Marshall, 1999: A model of decadal middle-latitude atmosphere–ocean coupled modes. *J. Climate*, **12**, 621–641.
- Gordon, C., C. Cooper, C. A. Senior, H. Banks, J. M. Gregory, T. C. Johns, J. F. B. Mitchell, and R. A. Wood, 2000: The simulation of SST, sea ice extents and ocean heat transports in a version of the Hadley Centre coupled model without flux adjustments. *Climate Dyn.*, **16**, 147–168.
- Grötzner, A., M. Latif, and T. P. Barnett, 1998: A decadal climate cycle in the North Atlantic Ocean as simulated by the ECHO coupled GCM. *J. Climate*, **11**, 831–847.
- Haarsma, R. J., F. M. Selten, J. D. Opsteegh, G. Lenderink, and Q. Liu, 1996: ECBILT: A coupled atmosphere ocean sea-ice model for climate predictability studies. KNMI Tech. Rep. TR-195, 32 pp. [Available from KNMI, P.O. Box 201, 3730 AE, De Bilt, Netherlands.]
- , —, and —, 2000: On the mechanism of the Antarctic Circumpolar Wave. *J. Climate*, **13**, 1461–1480.
- Hall, A., and S. Manabe, 1997: Can local linear stochastic theory explain sea surface temperature and salinity variability? *Climate Dyn.*, **13**, 167–180.
- Hasselmann, K., 1976: Stochastic climate models. Part I: Theory. *Tellus*, **28**, 473–485.
- James, I. N., and P. M. James, 1989: Ultra-low-frequency variability in a simple atmospheric model. *Nature*, **342**, 53–55.
- , and —, 1992: Spatial structure of ultra-low-frequency variability in the flow in a simple atmospheric circulation model. *Quart. J. Roy. Meteor. Soc.*, **118**, 1211–1233.
- Kushnir, Y., 1994: Interdecadal variations in North Atlantic sea surface temperature and associated atmospheric conditions. *J. Climate*, **7**, 141–157.
- , and I. M. Held, 1996: Equilibrium atmospheric response to North Atlantic SST anomalies. *J. Climate*, **9**, 1205–1220.
- Latif, M., and T. P. Barnett, 1996: Decadal climate variability over the North Pacific and North America: Dynamics and predictability. *J. Climate*, **9**, 1407–1423.
- Lau, N. C., and M. J. Nath, 1994: A modeling study of the relative roles of tropical and extratropical SST anomalies in the variability of the global atmosphere–ocean system. *J. Climate*, **7**, 1184–1207.
- Lenderink, G., and R. J. Haarsma, 1994: Variability and multiple equilibria of the thermohaline circulation associated with deep water formation. *J. Phys. Oceanogr.*, **24**, 1480–1493.
- Manabe, S., and R. J. Stouffer, 1996: Low-frequency variability of surface air temperature in a 1000-year integration of a coupled ocean–atmosphere model. *J. Climate*, **9**, 376–393.
- Marshall, J., and F. Molteni, 1993: Toward a dynamic understanding of planetary-scale flow regimes. *J. Atmos. Sci.*, **50**, 1792–1818.
- Mikolajewicz, U., and E. Maier-Reimer, 1990: Internal secular variability in an OGCM. *Climate Dyn.*, **4**, 145–156.
- Opsteegh, J. D., R. J. Haarsma, F. M. Selten, and A. Kattenberg, 1998: ECBILT, an atmospheric model of intermediate complexity: An alternative to mixed boundary conditions in ocean models. *Tellus*, **50**, 348–367.
- Palmer, T. N., 1999: A nonlinear dynamical perspective on climate prediction. *J. Climate*, **12**, 575–591.
- Reynolds, R. W., 1978: Sea surface temperature anomalies in the North Pacific Ocean. *Tellus*, **30**, 97–103.
- Rowell, D. P., 1998: Assessing potential seasonal predictability with an ensemble of multidecadal GCM simulations. *J. Climate*, **11**, 109–120.
- Saravanan, R., and J. C. McWilliams, 1997: Stochasticity and spatial resonance in interdecadal climate fluctuations. *J. Climate*, **10**, 2299–2320.
- , and —, 1998: Advective ocean–atmosphere interaction: An analytical stochastic model with implications for decadal variability. *J. Climate*, **11**, 165–188.
- Selten, F. M., R. J. Haarsma, and J. D. Opsteegh, 1999: On the mechanism of North Atlantic decadal variability. *J. Climate*, **12**, 1956–1973.
- Semtner, A. J., 1976: A model for the thermodynamic growth of sea-ice in numerical investigations of climate. *J. Phys. Oceanogr.*, **6**, 379–389.
- Tett, S. F. B., T. C. Johns, and J. F. B. Mitchell, 1997: Global and regional variability in a coupled AOGCM. *Climate Dyn.*, **13**, 303–323.
- Venzke, S., M. R. Allen, R. T. Sutton, and D. R. Rowell, 1999: The atmospheric response over the North Atlantic to decadal changes in sea surface temperature. *J. Climate*, **12**, 2562–2584.

- von Storch, J., V. Kharin, U. Cubasch, G. C. Hegerl, D. Schriever, H. von Storch, and E. Zorita, 1997: A 1260-year control integration with the coupled ECHAM1/LSG general circulation model. *J. Climate*, **10**, 1526–1544.
- Wallace, J. M., C. Smith, and Q. Jiang, 1990: Spatial patterns of atmosphere–ocean interaction in the northern winter. *J. Climate*, **3**, 990–998.
- Weaver, A. J., and E. S. Sarachik, 1991: Evidence for decadal variability in an ocean general circulation model: An advective mechanism. *Atmos.–Ocean*, **29**, 197–231.